The preparation of Ag_3BiBr_6 films and their preliminary use for solution processed photovoltaics

Jia Tu[1] · Chun Kou[1] · Meili Liu[1] · Hao Lu[2] · Yahui Liu[1] · Hongwei Tan[1] · Wenhua Li[1] · Zhishan Bo[1]

Abstract

Bismuth-halide-based perovskites could be promising candidates for construction of lead-free and air-stable perovskites solar cells. Herein we report a simple strategy on the fabrication of the Ag_3BiBr_6 thin films. They were prepared by flexible spin-coating procedure and the solvent of N-butylamine is found to be critical to dissolving AgBr precursor solution under lower room temperatures. Experiment and calculation analysis both reveal it with hexagonal structure. Their physical properties and photovoltaic performance were both characterized. We demonstrate that Ag_3BiBr_6 films are capable of storing stably over 30 days in air. These results will inspire more research works on developing and applying Ag_3BiBr_6 beyond solar energy applications.

Keywords Lead-free perovskite · Solar energy materials · Energy storage and conversion · Thin films

1 Introduction

Lead-halide perovskite solar cells (PSCs) have experienced a rapid development since 2009 [1], and their power conversion efficiencies (PCEs) have reached 23.3% in the past 9 years [2–7]. However, there are some serious issues with them, such as the toxicity of Pb and poor stability in humidity, which seriously restrict their further development towards commercial use [8–11]. Thus, Pb-free light absorbers have been diversely investigated over several years. For example, Grätzel replaced M of AMX_3 (the general formula of lead halide perovskites, A and M = 1 + and 2 + cations, respectively; X = Cl^-, Br^-, I^-) with Sn^{2+} and Ge^{2+} as they all belong to IVA group [11] and the PCE of $CH_3NH_3SnI_3$ has increased to 6%. Unfortunately, Sn^{2+} cation can be easily oxidized to Sn^{4+} and Ge^{2+} sensitive to air due to the low binding energy of its 4 s^2 electrons, [12–16],

causing their poor reproducibility. Hence, it is desirable to explore other elements to develop lead-free perovskites.

Bi^{3+} and Sb^{3+} feature close electronegativity and ionic radius comparable to Pb^{2+}. More importantly, bismuth halide perovskites exhibit mononuclear or polynuclear with corner-, edge- and/or face- sharing by connecting the adjacent bismuth halide octahedral [17, 18]. Bi- and Sb- based light absorbers like $A_3Bi_2I_9$, ABi_3I_{10}, $A_3Sb_2I_9$ (A = MA^+, Cs^+) and others have been studied in the light of advantages of Bi and Sb [19–22]. These combinations mostly show very low performance below 1% because of the poor charge transport property [23]. Therefore, heterovalent substitution of silver ions (Ag^+) for A was adopted to design Bi-based light absorbers with high-efficiency.

Such introduced Ag^+ can connect the neighboring iodobismuthate units, which show more intriguing properties theoretically [24]. Taking Cs_2AgBiX_6 (X = Br^-, Cl^-) with double perovskites structure as an example, the

---

✉ Wenhua Li, 11112013119@bnu.edu.cn; Zhishan Bo, zsbo@bnu.edu.cn | [1]Beijing Key Laboratory of Energy Conversion and Storage Materials, College of Chemistry, Beijing Normal University, Beijing 100875, China. [2]School of Materials Science and Engineering, Lanzhou University of Technology, Lanzhou 730050, China.

combination of monovalent and trivalent cation has been reported in it [25]. The band gap turns out to be indirect for most of these materials, and the indirect band gap would restrict them used as absorbers in single junction photovoltaic cells [26, 27]. Moreover, Ag^+ can replace Cs^+ completely and form a series of different $Ag_xBi_yI_z$ ($0 < x < 4$, $0 < y < 3$, $5 < z < 7$) compounds. For devices based on these compounds like $AgBi_2I_7$, Ag_2BiI_5 and Ag_3BiI_6, the best PCEs of 1.22%, 2.1% and 4.3% have been demonstrated, respectively [28–30], that comparable to other Pb-free PSCs. Meanwhile, their stability is obviously superior to the typical methylamine lead halides exposed in humid air. This signifies that silver-bismuth halide materials can be promising as potential candidates for fabrication of air-stable, lead-free PSCs. Noticeably, people mainly focus on the silver iodobismuthates materials as their relatively low E_g and high solubility at room temperature. In comparison, the bromide-based materials mostly have been limited to theoretical investigations. Both the structural and physical properties in experiment are yet reported neither the photovoltaic performance. The main constraint is due to the absence of solvent suitable to prepare precursor solution.

Herein, we report the utilization of n-butylamine to get a yellowish, homogeneous precursor solution. Furthermore, the Ag_3BiBr_6 perovskite material as film was made and its physical properties were demonstrated for the first time. Typically, the precursor solution with a mixture of silver bromide (AgBr) and bismuth bromide ($BiBr_3$) at molar ratio of AgBr:BiBr = 3:1 was spin-coated under ambient atmosphere subsequently with thermal annealing treatment. X-ray diffraction (XRD), computer calculations and energy-dispersive X-ray (EDX) spectrometry were used to identify the formation of Ag_3BiBr_6. We found that the obtained Ag_3BiBr_6 material has better thermal stability with decomposition temperatures up to 240 °C and also show inspiring stability over 30 days under ambient conditions by completely replacing I halogen. Specifically, we develop Ag_3BiBr_6 as light absorber to harvest solar energy by fabricating solar cells with the cell configuration (glass/fluorine-doped tin oxide (FTO) electrode/compact TiO_2/Ag_3BiBr_6/poly(3-hexylthiophene) (P3HT)/gold electrode). The best PCE of 0.033% for Ag_3BiBr_6 solar cells was preliminarily exhibited.

2 Experimental

Titanium tetra-iso-propanoate (TTIP, 97%, Sigma-Aldrich), 1-butanol (99.9%, Sigma-Aldrich), hydrochloric acid (36–38 wt% in water), silver bromide(AgBr, 99.998%, Alfa Aesar), bismuth(III) bromide ($BiBr_3$, 99%, Alfa Aesar), n-butylamine (99.0%, Alfa Aesar) and poly(3-hexylthiophene) (P3HT, One Material) were used as received without any purification.

Initially FTO coated glass substrates (15 × 20 mm, 15 Ω/cm^2 resistances) were etched with zinc powder and HCl (2 M). Then these FTO glass substrates were cleaned sequentially by ultrasonication in detergent, deionized water, acetone, and isopropanol for 20 min, respectively. Afterwards, FTO glasses were treated with an alkaline solution (with the volume ratio of H_2O:H_2O_2:NH_3 (aq) = 5:1:1) at 160 °C for 30 min, and then washed with deionized water several times to remove the residual alkaline solution. The compact TiO_2 layer was deposited by spin-coating 1.0 M titanium tetra(isopropanoate) 1-butanol solution (containing 1.0 M HCl) onto the FTO substrates at 3000 rpm for 60 s. Then the substrates were dried at 125 °C for 15 min to remove the solvent and sintered at 500 °C for 60 min [31]. After cooling down to room temperature, the perovskite layers were deposited by spin-coating the precursor solution (0.5087 mmol bismuth bromide and 0.2544 mmol silver bromide that dissolved in n-butylamine, 500 μL) at 3000 rpm for 60 s at room temperature. The precursor solution was stirred for 30 min to form clear, yellow solution before they were used. Then the substrates were heated at 150 °C for 30 min in air. The resulting film was then quenched to room temperature that was yellowish. For deposition of the hole transport layers, P3HT solution (15 mg/mL in 1,2-dichlorobenzene) was spin-coated at 2000 rpm for 30 s in ambient atmosphere and then coated substrates were further annealed at 100 °C for 15 min to remove the remaining solvent [20]. Finally, 80 nm of Ag was deposited by thermal evaporation on the top of the hole transport layer as the back contact under 10^{-6} mbar.

To determine the crystal structure of Ag_3BiBr_6, the unit cell parameters of Ag_3BiI_6 were adopted and I^- was replaced by Br^-. In details, the lattice constant in Ag_3BiBr_6 could be calculated by using the formula: $k = (r_{Br}^- + 3/4r_{Ag}^+ + 1/4r_{Bi}^{3+})/(r_I^- + 3/4r_{Ag}^+ + 1/4r_{Bi}^{3+})$ ($r_{Br}^- = 195$ pm, $r_I^- = 216$ pm, $r_{Bi}^{3+} = 108$ pm and $r_{Ag}^+ = 126$ pm). The theoretical XRD pattern of Ag_3BiBr_6 was calculated by Mercury 3.7 software (The Cambridge Crystallographic Data Centre, CCDC) based on the lattice constant. The calculated XRD pattern matches well with the experimental XRD pattern as we will discuss below, thus confirming the crystal structure of Ag_3BiBr_6.

The crystallographic properties of the perovskite thin films deposited on glass substrate were investigated by a Bruker X-ray diffractometer (XRD) with Cu Kα as the radiation source. The stability of Ag_3BiBr_6 films were tested in the ambient air, with a relative humidity of 50%. The UV–vis (ultraviolet–visible) absorption spectra were recorded by a PerkinElmer UV–vis spectrometer model Lambda 750. The glass substrate was measured as reference. PL (photoluminescence) spectra and time resolved

PL spectra of the fabricated thin films were obtained on PL spectrometer FLS 900 (Edinburgh Instruments). The emission for time resolved measurements was set at 463 nm. UPS (ultraviolet photoelectron spectroscopy) was recorded using a Kratos AXIS UTRADLD UPS/XPS system (Kratos analytical, Manchester, UK). The UPS measurement was carried out on an integrated ultra-high vacuum system (3.0×10^{-8} Torr) using the He(I) (21.22 eV) line in order to shift the spectra from the spectrometer threshold. The Ag_3BiBr_6 thin films for UPS measurement were prepared on silicon substrate. SEM (scanning electron microscope) images and EDX (energy dispersive X-Ray spectroscopy) data were obtained by S-4800 (Hitachi) field-emission scanning electron microscope (FESEM). The samples used for SEM and EDX measurements were fabricated on TiO_2/FTO/glass. Thermal gravimetric analysis (TGA) and differential scanning calorimetry (DSC) measurements were performed on TA2100 and Perkin-Elmer Diamond DSC instrument, respectively, under a nitrogen atmosphere at a heating rate of 10 °C/min. Powder samples of Ag_3BiBr_6 for TGA and DSC measurements were obtained by heating the stoichiometric ratio of precursors in n-butylamine in a Petri dish at 150 °C for about 4 h to remove completely the solvent.

The photovoltaic performance of the devices was measured using the Agilent B2902A Source Meter under the illumination of AM 1.5G (100 mW cm^{-2}) AAA class solar simulator (model XES-301S, SAN-EI) in nitrogen and the solar cells were masked with a black aperture to define the active area of 0.04 cm^2. The white light intensity was calibrated with a standard single-crystal Si solar cell.

3 Results and discussion

Compared with $BiBr_3$, the AgBr precursor is hardly soluble in polar aprotic solvents such as dimethylformamide (DMF) and dimethyl sulfoxide (DMSO), which tend to solubilize the metal halides. It is well-known that primary alkylamine groups ($R–NH_2$) are capable of solubilizing AgX ($X = I^-$, Br^- and Cl^-) [29], so we employed n-butylamine to prepare the precursor solution. Ag_3BiBr_6 films were deposited by spin-coating n-butylamine based precursor solution of AgBr and $BiBr_3$ (with the molar ratio of 3:1) on top of glass/FTO/TiO_2 substrate at room temperature of about 16 °C and subsequently annealing in an ambient atmosphere at 150 °C for 30 min. We found that the some small cracks were likely to appear on the surface of Ag_3BiBr_6 films while spin-coating at room temperature over 25 °C. This is probably due to the low boiling point of n-butylamine, and it easily evaporated from the film surface when films did not completely form yet. A scheme of the complete synthesis procedure is given in Scheme 1. The prepared film was
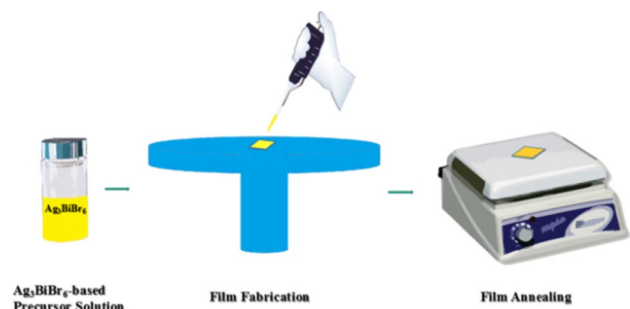
Scheme 1 Process for fabricating the Ag_3BiBr_6 films

firstly measured with single crystal X-ray diffractometer. In Fig. 1, there is no reference patterns present because it is not available in database. Fortunately, it is reasonable to propose that the patterns of Ag_3BiI_6 are similar to that of Ag_3BiI_6 [32]. Taking into account both the lattice parameters of Ag_3BiI_6 and the smaller radius of Br^- (195 pm) than I^- (216 pm), the corresponding lattice parameters of hexagonal Ag_3BiBr_6 were estimated as $a = b = 409.25(6)$ pm, $c = 1956.14(4)$ pm. The main crystallographic data of Ag_3BiBr_6 were demonstrated in Table 1. Bismuth and silver share octahedral sites with different mass ratio in the structure as showed in the Fig. 1a.

Based on this proposed lattice structure, we further simulated the XRD pattern for Ag_3BiBr_6 by using the Mercury 3.7 software. In Fig. 1b, both the experimental and calculated XRD patterns are exhibited. It is clear that these two patterns are consistent well with each other. In addition, the presence of $BiBr_3$ and/or AgBr can be excluded by comparing their diffraction peaks to Ag_3BiBr_6 (Figure S1), which confirms the successful formation of Ag_3BiBr_6. The formation of Ag_3BiBr_6 material can also be verified by EDX spectrometry (Figure S2). These results indicate that the obtained product is not simply a mixture of $BiBr_3$ and AgBr. The Ag_3BiBr_6 films are highly moisture- and air-stable for over 30 days, as is evident by the XRD pattern (Figure S3).

Thermo gravimetric analysis (TGA) and differential scanning calorimeter (DSC) were employed to test thermal stability of Ag_3BiBr_6. It is thermally stable up to 240 °C as inferred from the TGA and DSC data given in Fig. 2. TGA shows two step decomposition with the first step starting at around 240 °C associated with around 44% weight loss (loss of AgBr). The stability temperature of 240 °C is high enough for processing the material. There is no phase change observed in the range of 60–160 °C as DSC curve shown, which is a high enough range to operate solar cells, and these similar results were also observed in another study [32].

The optical bandgap of Ag_3BiBr_6 was calculated to be 2.58 eV according to the equation: $E_{gopt} = 1240/\lambda_{onset}$. The photoluminescence (PL) spectrum of Ag_3BiBr_6 is also shown in the inset, displaying a maximum emission at

Fig. 1 **a** Crystal structure of Ag$_3$BiBr$_6$ (space group R-3 m). **b** Calculated and experimental XRD patterns of Ag$_3$BiBr$_6$ film
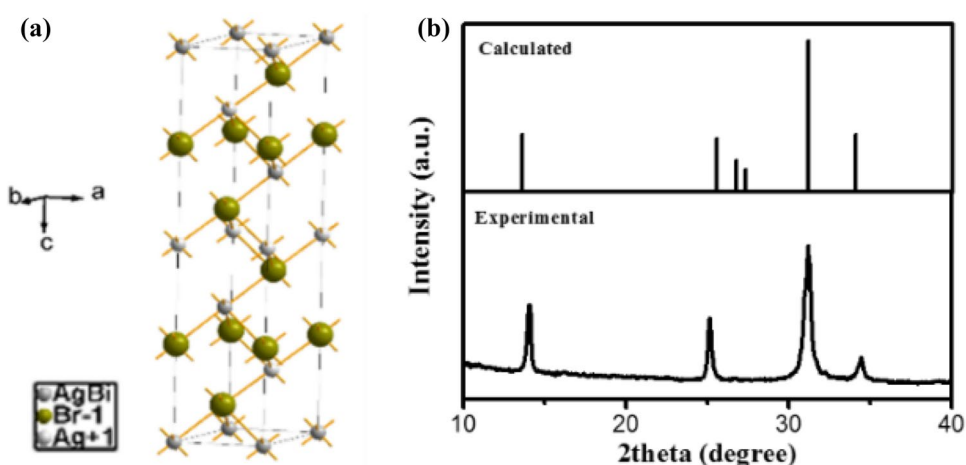

Table 1 Crystallographic data for Ag$_3$BiBr$_6$

Empirical formula	Ag$_3$BiBr$_6$
Formula weight	1012.10
Crystal system	Hexagona
Space group	R-3 m (166)
a = b, c (Å)	4.0925(6), 19.5614(4)
α, β, γ (°)	90, 90, 120
Volume (Å^3)	283.7
Z, ρ_{calcd} (g cm^{-3})	1

463 nm, with the Stokes shift of 63 nm. Fitting the curves with an exponential diffusion model results in the decay time of 0.81 ns for Ag$_3$BiBr$_6$ (Figure S4). Ultraviolet photoelectron spectroscopy (UPS) was used to study the electrochemical property of Ag$_3$BiBr$_6$. In Fig. 3b, the cutoff (E_{cutoff}) energy region of 16.45 eV and onset (E_{onset}) energy region of 1.41 eV are observed for Ag$_3$BiBr$_6$. Using the equations of $E_{HOMO} = 21.22 - (E_{cutoff} - E_{onset})$ and $E_{LUMO} = E_{HOMO} + E_g$, the HOMO energy level of -6.2 eV and LUMO of -3.6 eV can be deduced, respectively.

Fig. 2 **a** TGA and **b** DSC curves of Ag$_3$BiBr$_6$ under N$_2$ atmosphere
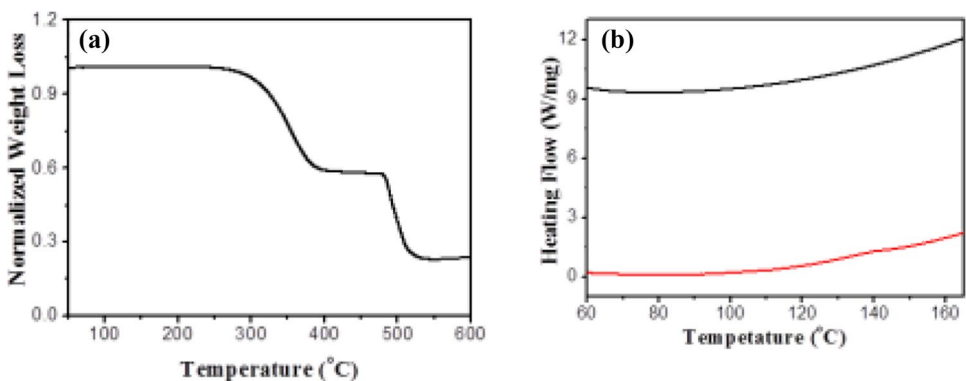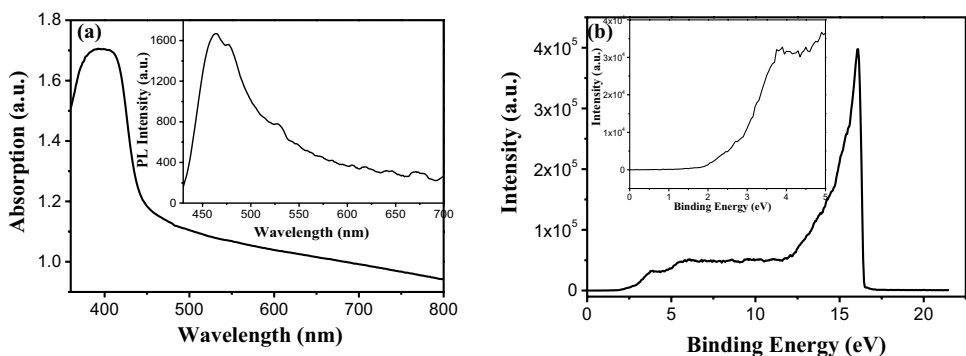

Fig. 3 **a** UV–vis absorption spectrum and the PL spectrum of Ag$_3$BiBr$_6$. **b** UPS spectrum in high binding-energy region of Ag$_3$BiBr$_6$ to determine the E_{cutoff} level (16.45 eV). The inset presents detail of the E_{onset} level (1.41 eV)

In view of the intrinsic properties investigated above, we fabricated Ag_3BiBr_6 based solar cells with the configuration (FTO) electrode/compact TiO_2/Ag_3BiBr_6/P3HT/ Ag electrode. Compact TiO_2 and P3HT are employed as electron transporting and hole transporting materials (ETM and HTM), respectively for our devices. The crystallized Ag_3BiBr_6 film annealed at 150 °C acts as the active layer and its surface morphology was characterized using scanning electron microscope (SEM) as shown in Fig. 4a. It reveals a basically continuous and fully-covered Film. Meanwhile, there are a spot of agglomerates observed in the films. This could be induced by the fast evaporation of n-butylamine with relative low boiling point during the spin-coating procedure. In Fig. 4b, each function layer of the prepared device could be clearly distinguished from the cross-sectional SEM image. An energy band diagram can be made referring to the relative energy levels discussed above. Wherein, the energy levels of TiO_2, P3HT, and Ag were obtained from literatures [20, 33, 34]. This implies that the charge transfer can successfully occur at the different interfaces for these devices (Fig. 4c).

To estimate the photovoltaic performance of these Ag_3BiBr_6-based devices, we measured the current density–voltage (J–V) characteristics of that fabricated under the optimal conditions. The J–V curves in Fig. 4d were obtained with a 20 ms scanning delay under standard air-mass 1.5 global (AM 1.5 G) illumination. It gives a short circuit current density (J_{SC}) of 0.12 mA/cm^2, open circuit voltage (V_{OC}) of 0.61 V and fill factor (FF) of 44.83%, resulting in a final PCE of 0.033%. In order to clarify the photovoltaic effect of Ag_3BiBr_6 material in these devices, we fabricated control devices without Ag_3BiBr_6 as well. As the J–V curve shown in Figure S5, the PCE is as low as less than 0.0005%. Therefore, Ag_3BiBr_6 could be a promising photoelectric material. Notably, there is almost no hysteresis behavior manifested in these Ag_3BiBr_6-based devices, indicating the Ag_3BiBr_6 films are of high quality without the large density of defects inside. Additionally, we tested many more devices and the corresponding performance parameters summarized in Table S1 testify the encouraging reproducibility of efficiency for devices. Besides, stability is also an important factor to evaluate the photovoltaic performance of solar cells. Accordingly, we investigated the stability of these Ag_3BiBr_6-based devices, and the PCE still maintains more than 95% of their initial efficiency after 7 days of exposure to ambient conditions without any encapsulation (Figure S6). Overall, even the PCE of Ag_3BiBr_6-based device is much lower than that of

Fig. 4 **a** Cross-sectional SEM image of the solar cell with the configuration of FTO/c-TiO_2/ Ag_3BiBr_6/P3HT/Ag. **b** Surface image of Ag_3BiBr_6 deposited on deposited on FTO/c-TiO_2. **c** Relative energy band diagram for Ag_3BiBr_6. **d** J–V curves in forward- and reverse-scan modes for Ag_3BiBr_6-based devices

	V_{oc} (V)	J_{sc} (mA cm^{-2})	FF	PCE (%)
Forward	0.61	0.12	44.83	0.033
Reverse	0.60	0.12	44.94	0.033
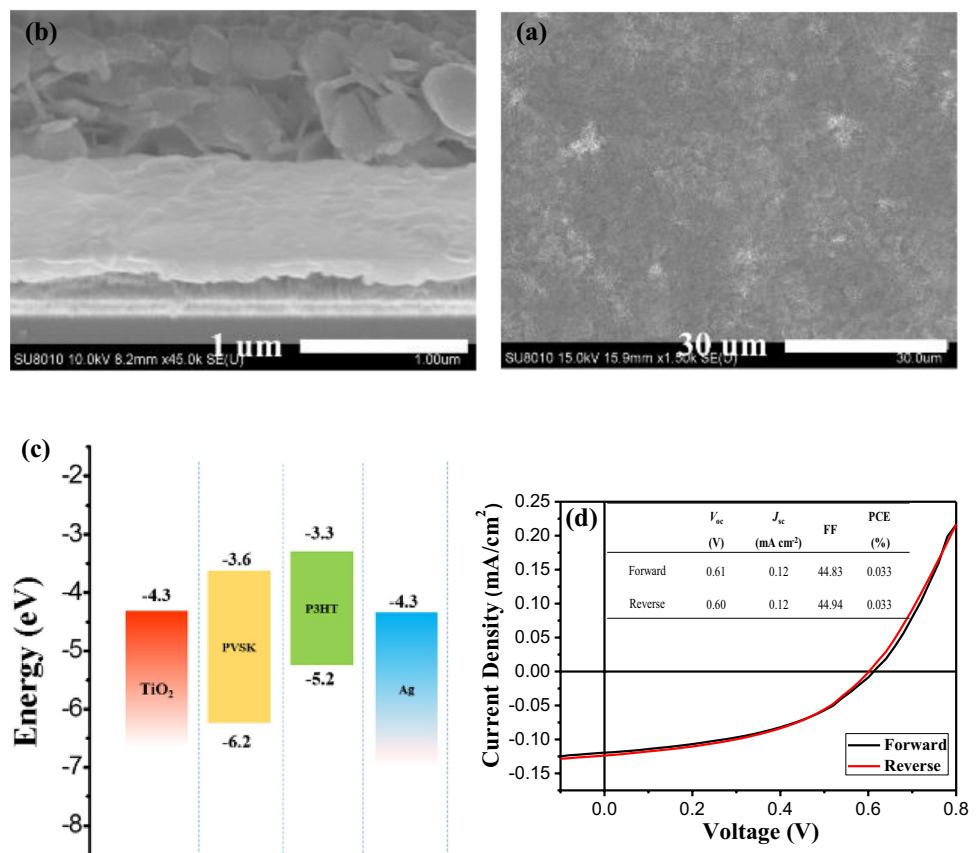
the other PSCs for the moment, the successful preparation of Ag_3BiBr_6 still extends the research field of photoelectric lead-free and stable materials.

4 Conclusion

In summary, the Ag_3BiBr_6 material and Ag_3BiBr_6-based PSCs were for the first time fabricated. We have demonstrated that solution-processed Ag_3BiBr_6 films were readily prepared using a flexible spin-coating method followed by a mild thermal annealing. Ag_3BiBr_6 is crystallized in the hexagonal perovskite phase, and the resulting Ag_3BiBr_6 is comparable to calculated XRD pattern. Ag_3BiBr_6-based PSCs yield a preliminary efficiency of 0.033% with relatively high V_{OC} of 0.61 V. The Ag_3BiBr_6-based solar cells is lead-free and air-stable. To optimize the Ag_3BiBr_6 films morphology may be an effective strategy for further improving the device performance. This is the first demonstration of Ag_3BiBr_6 light-absorbers for solar cell applications, which may inspire more research work to develop and use the material beyond for solar energy applications.

Compliance with ethical standards

Conflict of interest The authors declare that they have no conflict of interest.

References

1. Kojima A, Teshima K, Shirai Y, Miyasaka T (2009) Organometal halide perovskites as visible-light sensitizers for photovoltaic cells. J Am Chem Soc 131:6050–6051
2. Lee MM, Teuscher J, Miyasaka T, Murakami TN, Snaith HJ (2012) Efficient hybrid solar cells based on meso-superstructured organometal halide perovskites. Science 338:643–647
3. Burschka J, Pellet N, Moon S-J, Humphry-Baker R, Gao P, Nazeeruddin MK, Grätzel M (2013) Sequential deposition as a route to high-performance perovskite-sensitized solar cells. Nature 499:316
4. Liu M, Johnston MB, Snaith HJ (2013) Efficient planar heterojunction perovskite solar cells by vapour deposition. Nature 501:395
5. Jeon NJ, Noh JH, Kim YC, Yang WS, Ryu S, Seok SI (2014) Solvent engineering for high-performance inorganic–organic hybrid perovskite solar cells. Nat Mater 13:897
6. Saliba M, Matsui T, Seo J-Y, Domanski K, Correa-Baena J-P, Nazeeruddin MK, Zakeeruddin SM, Tress W, Abate A, Hagfeldt A, Grätzel M (2016) Cesium-containing triple cation perovskite solar cells: improved stability, reproducibility and high efficiency. Energy Environ Sci 9:1989–1997
7. NREL's "best research-cell efficiencies" chart. https://www.nrel.gov/pv/assets/pdfs/pv-efficiencies-07-17-2018.pdf. Accessed 18 July 2018
8. Babayigit A, Ethirajan A, Muller M, Conings B (2016) Toxicity of organometal halide perovskite solar cells. Nat Mater 15:47
9. Boix PP, Agarwala S, Koh TM, Mathews N, Mhaisalkar SG (2015) Perovskite solar cells: beyond methylammonium lead iodide. J Phys Chem Lett 6:898–907
10. Endres J, Kulbak M, Zhao L, Rand BP, Cahen D, Hodes G, Kahn A (2017) Electronic structure of the CsPbBr 3/polytriarylamine (PTAA) system. J Appl Phys 121:035304
11. Grätzel M (2014) The light and shade of perovskite solar cells. Nat Mater 13:838
12. Hao F, Stoumpos CC, Cao DH, Chang RPH, Kanatzidis MG (2014) Lead-free solid-state organic–inorganic halide perovskite solar cells. Nat Photonics 8:489
13. Kumar MH, Dharani S, Leong WL, Boix PP, Prabhakar RR, Baikie T, Shi C, Ding H, Ramesh R, Asta M, Graetzel M, Mhaisalkar SG, Mathews N (2014) Lead-free halide perovskite solar cells with high photocurrents realized through vacancy modulation. Adv Mater 26:7122–7127
14. Lee SJ, Shin SS, Kim YC, Kim D, Ahn TK, Noh JH, Seo J, Seok SI (2016) Fabrication of efficient formamidinium tin iodide perovskite solar cells through SnF2–pyrazine complex. J Am Chem Soc 138:3974–3977
15. Noel NK, Stranks SD, Abate A, Wehrenfennig C, Guarnera S, Haghighirad A-A, Sadhanala A, Eperon GE, Pathak SK, Johnston MB, Petrozza A, Herz LM, Snaith HJ (2014) Lead-free organic–inorganic tin halide perovskites for photovoltaic applications. Energy Environ Sci 7:3061–3068
16. Hu H, Dong B, Zhang W (2017) Low-toxic metal halide perovskites: opportunities and future challenge. J Mater Chem A 5:11436–11449
17. Hoefler SF, Trimmel G, Rath T (2017) Progress on lead-free metal halide perovskites for photovoltaic applications: a review. Monatshefte für Chemie Chem Mon 148:795–826
18. Lyu M, Yun J-H, Chen P, Hao M, Wang L (2017) Addressing toxicity of lead: progress and applications of low-toxic metal halide perovskites and their derivatives. Adv Energy Mater 7:1602512
19. Johansson MB, Zhu H, Johansson EM (2016) Extended photoconversion spectrum in low-toxic bismuth halide perovskite solar cells. J Phys Chem Lett 7:3467–3471
20. Lyu M, Yun J-H, Cai M, Jiao Y, Bernhardt PV, Zhang M, Wang Q, Du A, Wang H, Liu G, Wang L (2016) Organic–inorganic bismuth (III)-based material: a lead-free, air-stable and solution-processable light-absorber beyond organolead perovskites. Nano Res 9:692–702
21. Park BW, Philippe B, Zhang X, Rensmo H, Boschloo G, Johansson EM (2015) Bismuth based hybrid perovskites A3Bi2 I9 (A: methylammonium or cesium) for solar cell application. Adv Mater 27:6806
22. Saparov B, Hong F, Sun J-P, Duan H-S, Meng W, Cameron S, Hill IG, Yan Y, Mitzi DB (2015) Thin-film preparation and characterization of Cs3Sb2I9: a lead-free layered perovskite semiconductor. Chem Mater 27:5622–5632
23. Liang L, Gao P (2018) Lead-free hybrid perovskite absorbers for viable application: Can we eat the cake and have it too? Adv Sci 5:1700331
24. Chai W-X, Wu L-M, Li J-Q, Chen L (2007) Silver Iodobismuthates: syntheses, structures, properties, and theoretical studies of [Bi2Ag2I102-]n and [Bi4Ag2I162-]n. Inorg Chem 46:1042–1044
25. Greul E, Petrus ML, Binek A, Docampo P, Bein T (2017) Highly stable, phase pure Cs2AgBiBr 6 double perovskite thin films for optoelectronic applications. J Mater Chem A 5:19972–19981

26. Slavney AH, Hu T, Lindenberg AM, Karunadasa HI (2016) A bismuth-halide double perovskite with long carrier recombination lifetime for photovoltaic applications. J Am Chem Soc 138:2138

27. Savory CN, Walsh A, Scanlon DO (2016) Can Pb-free halide double perovskites support high-efficiency solar cells? ACS Energy Lett 1:949–955

28. Jung KW, Sohn MR, Lee HM, Yang IS, Sung SD, Kim J, Wei-Guang Diau E, Lee WI (2018) Silver bismuth iodides in various compositions as potential Pb-free light absorbers for hybrid solar cells. Sustain Energy Fuels 2:294–302

29. Kim Y, Yang Z, Jain A, Voznyy O, Kim GH, Liu M, Quan LN, Garcia de Arquer FP, Comin R, Fan JZ, Sargent EH (2016) Pure cubic-phase hybrid iodobismuthates $AgBi_2I_7$ for thin-film photovoltaics. Angew Chem 55:9586

30. Turkevych I, Kazaoui S, Ito E, Urano T, Yamada K, Tomiyasu H, Yamagishi H, Kondo M, Aramaki S (2017) Photovoltaic rudorffites: lead-free silver bismuth halides alternative to hybrid lead halide perovskites. ChemSusChem 10:3754–3759

31. Liu J, Wu Y, Qin C, Yang X, Yasuda T, Islam A, Zhang K, Peng W, Chen W, Han L (2014) A dopant-free hole-transporting material for efficient and stable perovskite solar cells. Energy Environ Sci 7:2963–2967

32. Harikesh PC, Mulmudi HK, Ghosh B, Goh TW, Teng YT, Thirumal K, Lockrey M, Weber K, Koh TM, Li S, Mhaisalkar S, Mathews N (2016) Rb as an alternative cation for templating inorganic lead-free perovskites for solution processed photovoltaics. Chem Mater 28:7496–7504

33. Kou C, Feng S, Li H, Li W, Li D, Meng Q, Bo Z (2017) Molecular "flower" as the high-mobility hole-transport material for perovskite solar cells. ACS Appl Mater Interfaces 9:43855–43860

34. Dong Y, Li W, Zhang X, Xu Q, Liu Q, Li C, Bo Z (2016) Highly efficient planar perovskite solar cells via interfacial modification with fullerene derivatives. Small 12:1098–1104

Publisher's Note Springer Nature remains neutral with regard to jurisdictional claims in published maps and institutional affiliations.